Temporal characterization of two-octave infrared pulses by frequency resolved optical switching

Adrien Leblanc, Adrien Longa, Mayank Kumar, Antoine Laramée, Charles Dansereau, Heide Ibrahim, Philippe Lassonde, François Légaré

Temporal characterization of two-octave infrared pulses by frequency resolved optical switching

Journal of Physics: Photonics

OPEN ACCESS

RECEIVED
13 April 2021

REVISED
12 July 2021

ACCEPTED FOR PUBLICATION
27 July 2021

PUBLISHED
27 August 2021

PAPER

Temporal characterization of two-octave infrared pulses by frequency resolved optical switching

Adrien Leblanc[1,2,*], **Adrien Longa**[1], **Mayank Kumar**[1], **Antoine Laramée**[1], **Charles Dansereau**[1], **Heide Ibrahim**[1], **Philippe Lassonde**[1] and **François Légaré**[1,*]

[1] Institut National de la Recherche Scientifique, Centre Énergie Matériaux et Télécommunications, 1650, Boulevard Lionel-Boulet, Varennes, Québec J3X 1S2, Canada
[2] Laboratoire d'Optique Appliquée, École Polytechnique, ENSTA, CNRS, Université Paris Saclay, Palaiseau, France
[*] Authors to whom any correspondence should be addressed.

E-mail: adrien.leblanc@ensta-paris.fr **and** francois.legare@inrs.ca

Keywords: temporal characterization, infrared pulse, supercontinuum, few-cycle pulse, optical parametric amplifier

Abstract

We present the temporal characterization of infrared pulses with spectra extending from 0.55 to 2.5 μm by using the frequency resolved optical switching (FROSt) technique. The pulses are obtained by broadening femtosecond pulses at 1.75 μm central wavelength in a two-stage hollow core fiber setup. This work demonstrates the capability of the FROSt technique to temporally characterize pulses with ultra-broadband spectra. Being free of phase-matching constraints, it enables the characterization of pulses with very low energy at the limit of the detection threshold and with arbitrary long pulse duration. This strength of the FROSt technique is illustrated by the characterization of supercontinua pulses whose spectra span over two octaves and with only 150 nJ energy that is spread temporally over almost 40 ps. The FROSt capabilities provide a versatile tool for the characterization of sub-cycle pulses and to study nonlinear processes such as supercontinuum generation.

1. Introduction

The generation and temporal characterization of single to sub-cycle laser pulses with high energy [1, 2] is motivated by the quests of generating attosecond x-ray pulses [3–5] and ultrashort electron bunches [6–8], for tracking ultrafast dynamics in atoms [9, 10], molecules [11, 12] and solids [13, 14]. Over the recent years, major efforts have been devoted to the development of technologies capable of generating and characterizing these pulses with spectra spanning over more than one octave of bandwidth [15]. Still, these tasks remain formidable challenges.

Regarding the generation of such ultrabroadband laser pulses, two main approaches have been developed. The ultra-broad spectral bandwidth is obtained either by the coherent combination of multiple optical parametric amplifiers (OPAs) [1, 16–20] derived from the same seed pulses, or by spectral broadening in a single optical arm by using a hollow core fiber (HCF) [21–25]. This latter method was demonstrated by employing a Ti:Sa system delivering 25 fs pulses at a central wavelength of 800 nm [26]. Due to the supercontinuum spectra, a single pair of chirped mirrors is not sufficient for chirp compensation over the whole bandwidth. Thus, a synthesizer was installed to divide the spectrum into different portions, each compressed with their respective chirped mirrors. Both compressed spectra are then coherently recombined. This approach enabled the generation of sub-millijoule sub-cycle light transients with spectra extending from the UV to the NIR spectral range [26, 27]. These pulses have been successfully used to generate isolated attosecond pulses, revealing, in turn, sub-fs electronic dynamics in silicon [28] and dynamics of the response of bound electrons in atoms [29]. In the same perspective, it was also proposed to use a HCF to broaden phase-locked signal and idler pulses derived from a single OPA [30]. These OPA-based approaches provide pulses at longer central wavelength and are thus ideal to scale the cut-off energy of photons obtained with high harmonic generation [5, 31, 32].

As technology enables the generation of supercontinua whose spectra span over broader ranges, advanced tools must be developed for their temporal characterization that remains very challenging. One such characterization approach consists in performing attosecond streaking measurements which requires the generation of attosecond pulses and detection of photoelectrons [17, 26]. This technique allows to retrieve both the attosecond pulses and the streaking field, i.e. the sub-cycle light transient. While it fulfills the requirements to characterize supercontinuum pulses, this technique is heavy to implement, requiring complex vacuum systems, XUV optics, and a photoelectron spectrometer. Recently, electro optical sampling was used to characterize the time-dependent electric field component of sub-cycle NIR-IR pulses [33]. Still, this requires measuring pulses shorter than the optical period of the characterized pulses, which imposes an additional technical challenge. In addition, these techniques are not practical if the pulse to be characterized is chirped to a large temporal duration as it requires scanning the pump-probe delay with accurate sampling steps over a large temporal window. Another promising approach free of phase matching constraints for the temporal characterization of ultra-broadband pulses is TIPTOE [34], but this technique is limited to pulses that are close to the Fourier transform-limited duration [35].

Alternatively, the temporal profiles of pulses spanning from the visible to the infrared spectral range have been characterized by adapted nonlinear optical techniques, such as frequency resolved optical gating (FROG) [36], spectral phase interferometry for direct electric field reconstruction (SPIDER) [37], or d-scan [38]. The mechanism at the core of these measurement techniques are frequency-mixing processes, such as sum frequency mixing (including second harmonic generation (SHG) FROG, cross correlation FROG, SPIDER, or d-scan) and four-wave mixing (including third harmonic generation FROG). All these techniques require phase-matching together with sufficient energy for the nonlinear optical process to occur. Therefore, in most cases they remain limited to the characterization of pulses whose spectra span over an octave of bandwidth [39–43] because fulfilling the phase matching condition requires very thin nonlinear crystals down to a few-μm thickness. In addition, the thinner the crystal, the more energy is required to obtain sufficient signal from the nonlinear process. Consequently, above one octave of bandwidth, it is very challenging to characterize the complete pulse at once. Note that recently two-octave spanning pulses were characterized with a technique based on sum-frequency mixing [44], the measurements required pulses with more than 500 μJ energy and close to the best compression.

We have recently developed the frequency resolved optical switching (FROSt) characterization technique based on transient absorption in solids [45]. A femtosecond pump pulse switches the transmissivity of a transparent material. The pulse to be characterized probes this ultrafast transmissivity drop and is frequency resolved as a function of the pump-probe delay. From the obtained spectrogram one can extract the temporal profiles in intensity and phase of both the switch function and the probe pulse with a phase retrieval algorithm. The bandwidth of the measurement is only restricted by the transparency window of the photoexcited switch material, thus enabling to characterize pulses in the visible to mid-IR spectral region. For instance, different window materials should allow the characterization of spectra extending from 2 to 20 μm using germanium, 1 to 15 μm using silicon, or 0.5 to 20 μm using zinc selenide (ZnSe). In our previous work [45], several few-cycle pulses centered at 0.8, 1.7, 4 and 10 μm were characterized. Note that a similar approach was already used in [46, 47] where the reflectivity of a sample was switched by a pump pulse and probed by the pulse to be characterized. However, the technique proposed in these cases only enables to evaluate the chirp of the probe pulses, rather than a complete pulse characterization. Another technique, very similar to the FROSt, is based on the generation of a plasma mirror (PM) to induce an ultrafast reflectivity switch of a material. It is termed the PM FROG [48, 49]. The use of a PM provides the advantage to enable the characterization with an optical gating technique of pulses down to the ultraviolet spectral range. However, this technique requires a complex setup with a vacuum chamber, and requires tight focusing of the pump pulses to generate the plasma which involves a more complex alignment procedure, thus it is not intended to characterize pulses from the visible to the mid-IR spectral range.

In this work, we take advantage of a FROSt property which is that the measured signal is directly the spectrum of the output pulse transmitted through the switch material. Therefore, the amount of detected signal is insensitive to the temporal spread of the pulse to be characterized, enabling to measure pulses from Fourier transform limited (FTL) to pulses with large amounts of chirp. This is demonstrated here by characterizing one-octave spanning pulses dispersed in different materials both by FROSt and SHG-FROG. While low energy pulses (only a few-100 nJ) are characterized by FROSt, the pulse energy must be adapted for each SHG-FROG characterization and significantly increased (up to more than 100 μJ) to provide enough signal for the measurement when the pulse duration is long (a few-ps). Then, we show the capability of FROSt to characterize supercontinua whose spectra span over more than two octaves from 0.55 to 2.5 μm. With only 150 nJ energy, they are temporally spread by propagation in different dispersive materials up to

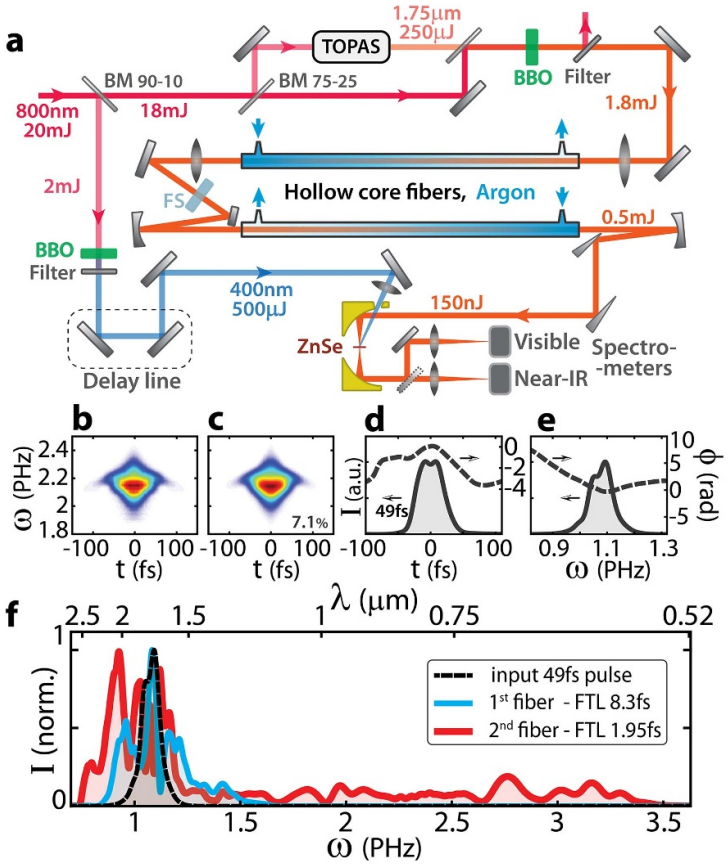

Figure 1. (a) Layout of the experimental setup. In the first arm, the 800 nm pulses are converted to 1.75 μm pulses with the use of a commercial OPA (TOPAS, Light Conversion) and an additional home-built OPA stage (2 mm-thick type II BBO crystal). The pulses are spectrally broadened with two consecutive HCFs. For the FROSt measurements, a few-100 nJ of pulse energy are selected by reflections from wedges. In the other arm with a delay line, 2 mJ of the 800 nm beam are selected and frequency doubled to pump the ZnSe plate for the FROSt characterization. For this measurement, the ZnSe window is placed near the focus of a confocal setup composed of two parabolic mirrors. A flip mirror selects either the visible/near-IR or the near-IR/IR spectrometer. (b)–(e) SHG-FROG characterization of the near-IR pulses at the entrance of the first fiber. Measured and reconstructed SHG-FROG spectrograms in panels (b) and (c), with the reconstruction error calculated as in [45]. Temporal (panel (d)) and spectral (panel (e)) profiles of the pulse in intensity (full line) and phase (dash line). (f) Intensity spectra of the pulses before the first fiber (dashed black line), after the first fiber (blue solid line), and after the second fiber (red solid line). These two latter spectra support a bandwidth of respectively 8.3 and 1.95 fs FTL.

almost 40 ps resulting in a very low average power of only ~4 pJ fs^{-1}. Such ultra-broadband pulses with very low energy and very long duration would have been very challenging to characterize by any other mean. This work demonstrates the strengths of FROSt to be a versatile and practical tool for studies requiring supercontinua pulses.

2. Methods

2.1. Experimental setup

The experiments were carried out at the advanced laser light source laboratory located at INRS-EMT (Varennes, Canada). A layout of the experimental setup is presented in figure 1(a). A 50 Hz Ti:Sa laser system delivering femtosecond pulses with 20 mJ of energy at a central wavelength of 800 nm is used for this experiment. A small part of this energy, about 4.5 mJ, is used to pump a commercial OPA (TOPAS, Light Conversion) to obtain seed pulses at 1.75 μm. The main part of the 800 nm pulse energy is used to further amplify these 1.75 μm pulses from ~250 μJ to an energy of 1.8 mJ with a home built OPA stage [21]. The pulse duration is measured to 49 fs full width at half maximum (FWHM) of peak intensity by SHG-FROG, see figures 1(b)–(e).

A cascade of two 2 m long HCFs (*few-cycle* Inc.) with 1 mm inner diameter is used for spectral broadening. The first fiber is filled with argon in a differential pumping configuration with a supply pressure of 1 atm at the output and a primary vacuum at the input. At the output of the first HCF, the 1.75 μm pulses

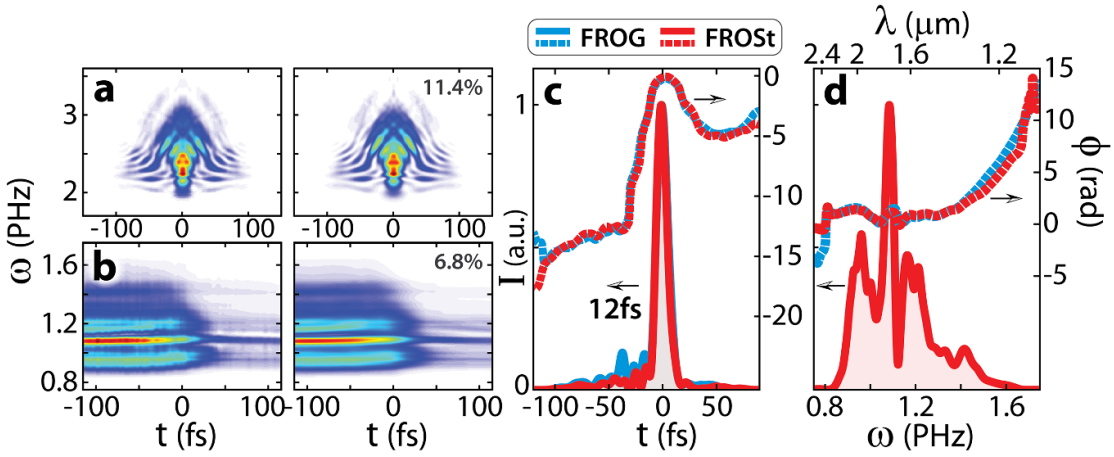

Figure 2. SHG-FROG and FROSt characterization of the one octave spanning pulses at the output of the first fiber. (a) Measured FROG spectrogram (left panel) and reconstructed FROG spectrogram (right panel) with a ptychographic algorithm as in [45]; the reconstruction error of the retrieved spectrogram compared to the experimental one, evaluated as in [45], is written in percentage in the right panel. (b) Similarly as panels (a), measured (left panel) and reconstructed (right panel) FROSt spectrograms with the reconstruction error in the right panel. (c), (d) Temporal, panel (c), and spectral, panel (d), profiles of the pulse in intensity (full lines) and phase (dashed lines) retrieved from the FROG (blue lines) and the FROSt (red lines) measurements. At the top of the panel (d) is added the spectral axis in wavelengths.

have an energy of ∼1 mJ and their spectra extend from 1.15 to 2.2 μm, see figure 1(f), with 8.3 fs FTL duration. They are compressed down to ∼12 fs by propagation through a 5 mm thick fused silica (FS) window [50], two independent temporal characterization measurements are shown in figure 2 (details on the measurements are provided further). The second fiber is filled with a supply pressure of 1.2 atm of argon in a similar differential pumping configuration. At the output of the second HCF, the pulse energy is ∼490 μJ and the pulses exhibit wide spectral broadening with spectra spanning from 0.55 to 2.5 μm, see figure 1(f), corresponding to a FTL duration of 1.95 fs. Note that two spherical mirrors (1 m focal length) are used for coupling the beam at the entrance of the second fiber and for collimating the beam at its output, in order to prevent from adding spectral dispersion to the pulses, as it would occur with lenses. The whole spectrum is obtained in two consecutive measurements with two spectrometers by using a flip mirror: a visible/near-IR (USB2000, Ocean Optics) and a near-IR/IR spectrometer (NIR256-2.1, Ocean Optics) measure the spectra respectively from 0.5 to 1.17 and from 0.84 to 2.57 μm. The overlapping spectral windows (i.e. from 0.84 to 1.17 μm) enables to precisely adjust both signal levels to concatenate spectra spanning over the full spectral range. The central wavelength, defined as the wavelength separating the spectrum in two parts of equal energy, is 1.65 μm (1.15 PHz).

The SHG-FROG and the FROSt measurements of the compressed octave spanning pulses at the output of the first HCF are presented in figure 2. Dispersion compensation was performed using linear propagation in 5 mm thick FS window. The FROG setup is homebuilt and the SHG signal is obtained with a type-I beta barium borate (BBO) crystal whose thickness is 10 μm. The FROSt measurements are obtained by switching the optical transmissivity of a 500 μm thick ZnSe plate with pump pulses of ∼70 fs duration, ∼500 μJ energy, and 400 nm central wavelength. These pump pulses are derived from the SHG of the 800 nm sampled at the output of the compressor of the Ti:Sa beamline, see figure 1(a). They are focused onto the ZnSe plate by a lens with 15 cm focal length. The ZnSe plate is placed approximately 1.5 cm before the focus of the pump beam to obtain a beam size of ∼1 mm at the surface. Note that it is placed before the pump focus, and not after, in order to avoid nonlinear effects in air (at the pump focus, the intensity would be of a few-10^{15} W cm^{-2}). The 1.75 μm pulses are attenuated to ∼300 nJ by the reflection of three wedges and are focused with a 10 cm off-axis parabola onto the ZnSe plate at the center of the pump focal spot. The corresponding fluences of both interacting beams are estimated for the pump and probe beams to respectively 70 and 1 mJ cm^{-2}. After propagation through the photoexcited ZnSe plate, the pulses are focused into the spectrometer with a 10 cm focal lens and are frequency resolved as a function of their relative delay with the pump pulses.

2.2. Comparison of the FROSt and the FROG techniques

The FROG and FROSt measurements of the 12 fs pulses are presented in figure 2. The temporal (panel c) and spectral (panel d) profiles retrieved by both techniques are very similar. Pulse durations of 12.2 fs and 11.7 fs FWHM are obtained respectively, corresponding to two optical cycles at 1.75 μm.

Table 1. Summary of the fluences on the BBO crystal or on the ZnSe window times the number of accumulated shots per delay to provide an equivalent signal for the SHG-FROG or the FROSt characterizations or the one octave pulses propagated through different materials.

	Compressed pulse, figures 2(a) and (b)	FS 10 mm, figures 5(a) and (b)	FS 35 mm, figures 5(e) and (f)	ZnSe 12 mm, figures 5(i) and (j)	ZnSe 20 mm, figures 5(m) and (n)
Energy spread	A few-10 fs	∼300 fs	∼1 ps	∼3 ps	∼5.5 ps
SHG-FROG	1.5 mJ cm^{-2} × 1 shot	1.5 mJ cm^{-2} × 2 shots	15 mJ cm^{-2} × 2 shots	60 mJ cm^{-2} × 6 shots	60 mJ cm^{-2} × 20 shots
FROSt	1 mJ cm^{-2} × 1 shot	1 mJ cm^{-2} × 1 shot	1 mJ cm^{-2} × 1 shot	1 mJ cm^{-2} × 1 shot	1 mJ cm^{-2} × 1 shot

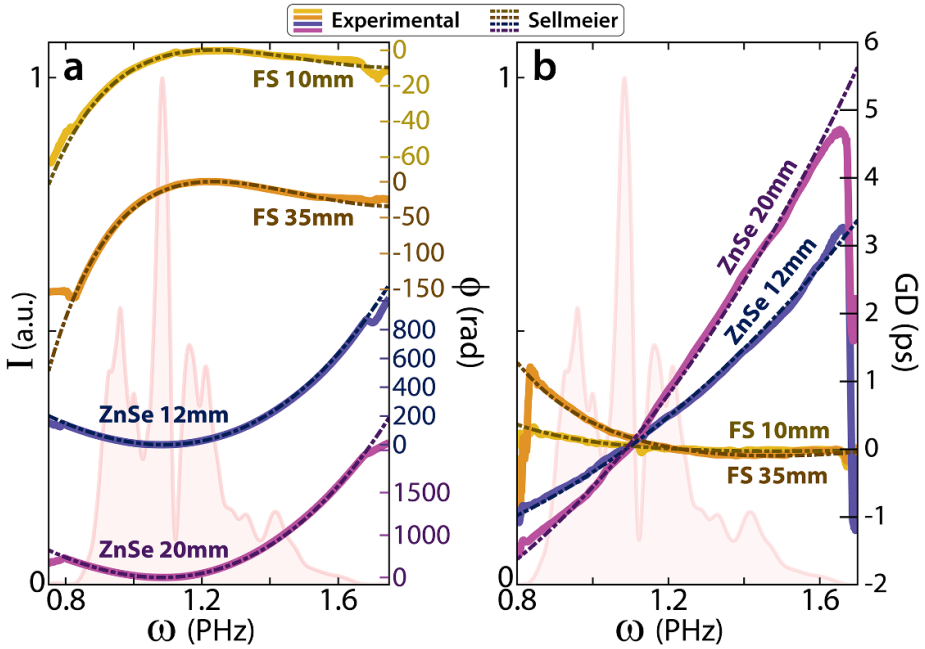

Figure 3. (a) Spectral dispersion added by the different material windows calculated theoretically by the Sellmeier equations and experimentally by the difference of spectral phase between the pulse propagated through the windows of FS whose thicknesses are 10, from figure 5(d), or 35 mm, from figure 5(h), or through the windows of ZnSe whose thicknesses are 12, from figure 5(l), or 20 mm, from figure 5(p), to the initial 12 fs pulse's spectral phase, from figure 2(d). (b) Deduced spectral profiles of the GD for each window in picoseconds, calculated by $GD(\omega) = d\phi(\omega)/d\omega$.—Note that the panel (b) is slightly zoomed along the spectral axis compared to panel (b). The pulse spectrum is illustrated in light red line in both panels.

Note that while both the SHG-FROG and the FROSt spectrograms encode the same information (the amplitude and phase profile of the pulse) which can be extracted with a phase retrieval algorithm, they exhibit very different features. In figure 2(a), the FROG signal, arising from a SHG process, is at maximum at zero delay, i.e. when both pulse replicas interact in the BBO crystal at the same time. The SHG signal decreases down to zero for long delays (symmetrically in the positive and negative delays). On the contrary, the FROSt spectrogram is not symmetrical (see figure 2(b)). For long negative delays, the probe pulse to be characterized propagates through the sample far before the pump pulse, therefore the sample is not yet photo-excited, thus transparent for the probe pulse, and the measured signal is directly the probe pulse spectrum. For long positive delays, the pump pulse interacts with the sample far before the probe pulse which thus probes an opaque window and do not propagates through it; the output signal is very low. This explains the asymmetric shape of the FROSt spectrogram and why this technique is sensitive to the absolute value of the spectral phase as opposed to SHG-FROG. More information can be found in [45].

To demonstrate the flexibility of FROSt to characterize pulses with arbitrary long duration, spectral phase is added to the probe pulses by linear propagation in different dispersive media (FS and ZnSe). The FROSt measurements are compared to SHG-FROG ones, see figure 5 in the appendix. As the pulse energy is temporally spread, the FROG setup is slightly modified for each measurement to optimize the SHG signal: the more the pulse energy is spread in time, the more fluence on the BBO crystal is required to detect the SHG signal. An iris selects a part of the beam to be characterized at the entrance of the FROG setup, the beam is then split with a d-shape mirror in two parts of equal energy whose relative delay is controlled accurately with a motor. Finally, both parts are focused with a spherical mirror of 15 cm focal onto the BBO

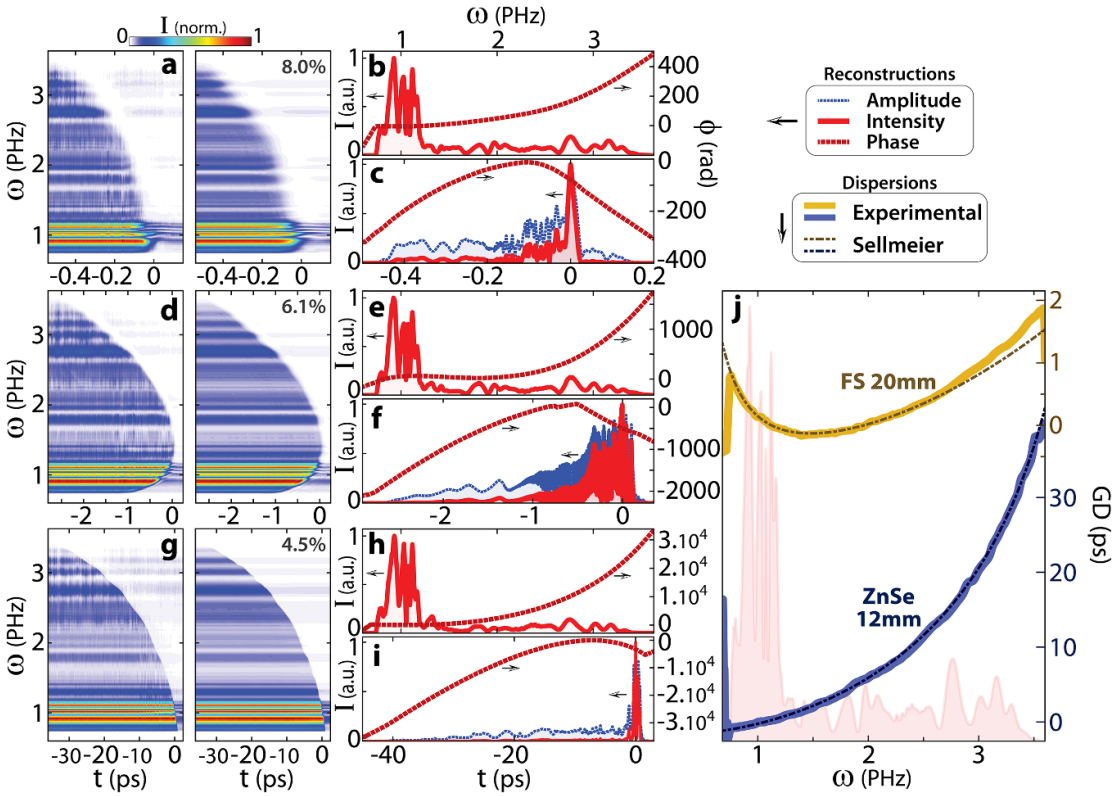

Figure 4. FROSt measurements of the two-octave spanning supercontinua after the second HCF. First and second columns, experimental and reconstructed FROSt spectrograms with the reconstruction error evaluated as in [45] . Retrieved spectral profiles in intensity (full lines) and phase (dashed lines) in panels (b), (e), and (h). Retrieved temporal profiles in amplitude (dashed blue lines), intensity (full red lines) and phase (dashed red lines) in panels (c), (f) and (i). The pulses at the output of the second HCF, panels (a) to (c), are dispersed by propagation through a FS window whose thickness is 20 mm, panels (d) to (f), or through a ZnSe window whose thickness is 12 mm, panels (g) to (i). In panel (j) are presented the spectral profiles of the GD in picoseconds added by the different windows calculated theoretically by the Sellmeier equations and experimentally by the derivative of the difference of spectral phase between the pulse propagated through the windows of FS, from panel (e), or of ZnSe, from panel (h), compared to the initial pulse's spectral phase, from panel (b).

crystal with a 4° relative angle. The output harmonic signal at the center of the two output fundamental beams is focused with a 10 cm focal lens into the visible/near-IR spectrometer. For the 12 fs pulse characterization shown in figure 2(a), the iris diameter is set to ∼2 mm to select 20 μJ out of the 1 mJ pulses (∼14 mm diameter beam). The fluence on the BBO crystal is estimated to ∼1.5 mJ cm^{-2}. The spectrogram is obtained by integrating the harmonic signal during 20 ms (one shot at 50 Hz). To provide the same signal level when the pulse is spectrally dispersed by propagation through a 10 mm FS window, figure 5(a), the signal is integrated over 40 ms (two shots). For the other measurements, to obtain an equivalent signal level, the entrance iris was opened to select more input energy. After propagation through windows of FS of 35 mm thickness, and of ZnSe of 12 and 20 mm thicknesses, the input energy into the FROG setup was respectively 60 (FS case) and 120 μJ (ZnSe cases), with estimated fluences on the BBO crystal of 15 and 60 mJ cm^{-2}, see figures 5(e), (i), and (m). In addition, the signal is integrated during 40, 120, and 400 ms respectively, i.e. 2, 6, and 20 shots. On the contrary, for the five different FROSt measurements, the setup is exactly the same: no optimization is required as the measured signal is directly the output pulse spectrum which does not involve any nonlinear wavelength conversion. The estimated pulse fluences on the BBO crystal (FROG) or ZnSe plate (FROSt) and the number of shots required to obtain the same signal levels for the different measurements is summarized in the table 1.

Note that these results must be also compared to the fluence of the pump pulses onto the ZnSe plate used for the FROSt measurements: 70 mJ cm^{-2} × 1 shot. The main drawback of the FROSt technique is that an intense pump pulse is required to perform the measurement, here 500 μJ per pulse. However, the measurement could have been performed with less energy in the pump beam, down to a few-10 μJ, by setting the position of the ZnSe plate closer to the pump focus in order to keep a similar level of fluence. In addition, in many optical systems based on OPAs, an intense pump beam is available. As soon as such a pulse is available to perform the measurement, the results summarized in table 1 show that the characterization is

not affected by the temporal duration of the pulse to be characterized, enabling to measure highly chirped pulses.

As observed in figure 5, the pulse intensity and phase profiles retrieved by FROG and FROSt exhibit the same features. To further demonstrate the quality of the reconstructions, the spectral phases induced by the different dispersive windows are compared to the dispersion predicted from the Sellmeier equations in figure 3(a). The theoretical spectral phase is verified by the experimental measurements. In addition, the spectral profiles of the group delay (GD) induced by each window, deduced from the expression $\mathrm{GD}(\omega) = \mathrm{d}\Phi(\omega)/\mathrm{d}\omega$, are presented in figure 3(b). These GDs provide an intuitive perception of how the pulses are stretched by propagation through the windows.

2.3. Supercontinuum characterization

After such cross-check of the reliability of the FROSt technique for the current experimental condition, we now turn to the characterization of the supercontinuum pulses at the output of the second fiber. This is performed with the same FROSt setup. An energy of 150 nJ is selected out of the available 490 μJ by the reflection off three wedges. The pulse fluence on the ZnSe plate is estimated to 0.5 mJ cm^{-2}. The pulses span over more than two octaves from a pulsation of 0.75–3.6 PHz (i.e. from a wavelength of 0.55–2.5 μm), equivalent to 2.25 octaves. The pulse duration is 450 fs at $1/e^2$ in intensity and its energy spreads over $\sim$600 fs, figure 4(c).

To further validate the reconstructions, spectral phase is added to the pulse by linear propagation in a FS window of 20 mm thickness, figures 4(d)–(f), and a ZnSe window of 12 mm thickness, figures 4(g)–(i). In the latter case, as can be observed in panel (i), the supercontinuum energy is temporally spread over almost 40 ps. The pulse average power is estimated to $\sim$4 pJ fs^{-1}. Finally, the theoretical spectral profiles of the GDs added by propagation through the FS and the ZnSe windows (and calculated by the Sellmeier equations) are verified experimentally over the whole bandwidth, see figure 4(j).

3. Conclusions

In conclusion, we have demonstrated the capability of the FROSt technique to temporally characterize pulses with two more than octaves of bandwidth, spanning from the visible to the near infrared spectral range from 0.55 to 2.5 μm. The pulses were generated using a standard commercial Ti-Sa pumped OPA, and a cascade of two HCFs. Exploiting the phase-matching free property of FROSt, this technique has proven its flexibility by the characterization, with the same setup, of different one-octave bandwidth pulses whose energy temporally spreads over a few-10 fs to a few-ps. In the same conditions, a characterization technique based on a nonlinear process such as SHG-FROG must be optimized for each pulse and is limited for highly chirped pulses for which the average power becomes too low for the nonlinear effect to produce a sufficient signal. Finally, a pulse with 150 nJ energy, two-octave bandwidth, and with an energy spread over almost 40 ps is characterized by FROSt. Based on these results, FROSt appears as a promising technique to characterize low energy pulses obtained from supercontinuum generation in advanced waveguides [51].

Data availability statement

The data that support the findings of this study are available upon reasonable request from the authors.

The data generated and/or analyzed during the current study are not publicly available for legal/ethical reasons but are available from the corresponding author on reasonable request.

Appendix

Figure 5 shows the SHG-FROG and the FORSt measurements and reconstructions of the one octave pulses at the output of the first HCF that were propagated through different material windows. From these reconstructions were deduced the experimental curves presented in figure 3.

Note that most differences between the profiles retrieved by the FROG and the FROSt techniques arise from the low energy spectral components that are in the wings of the spectrum. These differences in the retrieved spectral phase profiles produce slight changes in the retrieved temporal profile. As the SHG-FROG relies on a second order nonlinear process, a high dynamic range is required to observe in the FROG spectrogram the SHG signal that arises from the low energy spectral components. Even with the high-dynamic range of our spectrometer (NIR256-2.1, Ocean Optics), it is likely that some of the SHG signal is at the noise level in the spectrograms (see figures 5(a), (e), (i), (m)).

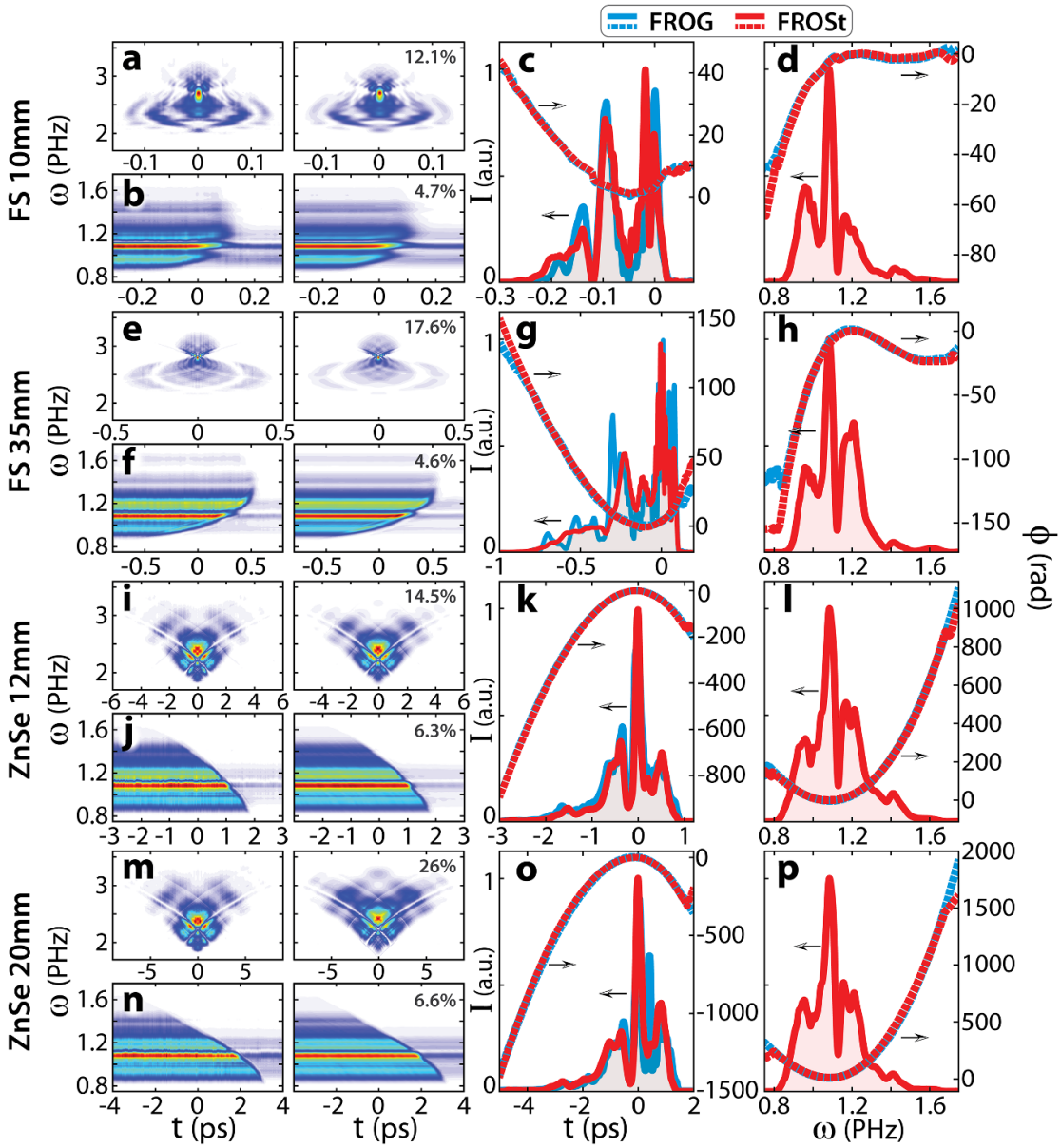

Figure 5. SHG-FROG and FROSt characterization of the one octave spanning pulses at the output of the first fiber. First and second columns, measured and reconstructed FROG (panels (a), (e), (i), (m)) and FROSt (panels (b), (f), (j), (n)) spectrograms, with the reconstruction error evaluated as in [45]. Third column, temporal profiles of the pulse in intensity (full lines) and phase (dashed lines) retrieved from the FROG (blue lines) and the FROSt (red lines) measurements. Fourth column, pulses spectra in full red lines together with the retrieved spectral phase profiles from the FROG (dashed blue lines) and FROSt (dashed red lines) measurements. The pulse from figure 2 is propagated through windows of FS whose thicknesses are 10 and 35 mm in panels (a) to (d) and (e) to (h), and windows of ZnSe whose thicknesses are 12 and 20 mm in panels (i) to (l) and (m) to (p).

ORCID iDs

Adrien Leblanc https://orcid.org/0000-0002-5894-6611
Mayank Kumar https://orcid.org/0000-0002-9237-1567
Heide Ibrahim https://orcid.org/0000-0001-6371-8501

References

[1] Huang S-W *et al* 2011 High-energy pulse synthesis with sub-cycle waveform control for strong-field physics *Nat. Photon.* **5** 475–9
[2] Hentschel M, Kienberger R, Spielmann C, Reider G A, Milosevic N, Brabec T, Corkum P, Heinzmann U, Drescher M and Krausz F 2001 Attosecond metrology *Nature* **414** 509–13
[3] Christov I P, Murnane M M and Kapteyn H C 1997 High-harmonic generation of attosecond pulses in the "single-cycle" regime *Phys. Rev. Lett.* **78** 1251
[4] Sansone G *et al* 2006 Isolated single-cycle attosecond pulses *Science* **314** 443–6

[5] Popmintchev T *et al* 2012 Bright coherent ultrahigh harmonics in the keV x-ray regime from mid-infrared femtosecond lasers *Science* **336** 1287–91
[6] Schmid K *et al* 2009 Few-cycle laser-driven electron acceleration *Phys. Rev. Lett.* **102** 124801
[7] Ouillé M *et al* 2020 Relativistic-intensity near-single-cycle light waveforms at kHz repetition rate *Light Sci. Appl.* **9** 47
[8] Payeur S, Fourmaux S, Schmidt B E, MacLean J P, Tchervenkov C, Légaré F, Piché M and Kieffer J C 2012 Generation of a beam of fast electrons by tightly focusing a radially polarized ultrashort laser pulse *Appl. Phys. Lett.* **101** 041105
[9] Goulielmakis E *et al* 2010 Real-time observation of valence electron motion *Nature* **466** 739–43
[10] Holler M, Schapper F, Gallmann L and Keller U 2011 Attosecond electron wave-packet interference observed by transient absorption *Phys. Rev. Lett.* **106** 123601
[11] Sansone G *et al* 2010 Electron localization following attosecond molecular photoionization *Nature* **465** 763–6
[12] Calegari F *et al* 2014 Ultrafast electron dynamics in phenylalanine initiated by attosecond pulses *Science* **346** 336–9
[13] Cavalieri A L *et al* 2007 Attosecond spectroscopy in condensed matter *Nature* **449** 1029–32
[14] Siegrist F *et al* 2019 Light-wave dynamic control of magnetism *Nature* **571** 240–4
[15] Manzoni C, Mücke O D, Cirmi G, Fang S, Moses J, Huang S-W, Hong K-H, Cerullo G and Kärtner F X 2015 Coherent pulse synthesis: towards sub-cycle optical waveforms *Laser Photonics Rev.* **9** 129–71
[16] Manzoni C, Huang S-W, Cirmi G, Farinello P, Moses J, Kärtner F and Cerullo G 2012 Coherent synthesis of ultra-broadband optical parametric amplifiers *Opt. Lett.* **37** 1880–2
[17] Rossi G M, Mainz R E, Yang Y, Scheiba F, Silva-Toledo M A, Chia S-H, Keathley P D, Fang S, Mücke O D and Manzoni C 2020 Sub-cycle millijoule-level parametric waveform synthesizer for attosecond science *Nat. Photon.* **14** 629–35
[18] Alismail A, Wang H, Barbiero G, Altwaijry N, Hussain S A, Pervak V, Schweinberger W, Azzeer A M, Krausz F and Fattahi H 2020 Multi-octave, CEP-stable source for high-energy field synthesis *Sci. Adv.* **6** eaax3408
[19] Liang H *et al* 2017 High-energy mid-infrared sub-cycle pulse synthesis from a parametric amplifier *Nat. Commun.* **8** 1–9
[20] Schmidt B E, Thiré N, Boivin M, Laramée A, Poitras F, Lebrun G, Ozaki T, Ibrahim H and Légaré F 2014 Frequency domain optical parametric amplification *Nat. Commun.* **5** 3643
[21] Cardin V, Thiré N, Beaulieu S, Wanie V, Légaré F and Schmidt B E 2015 0.42 TW 2-cycle pulses at 1.8 μm via hollow-core fiber compression *Appl. Phys. Lett.* **107** 181101
[22] Sollapur R *et al* 2017 Resonance-enhanced multi-octave supercontinuum generation in antiresonant hollow-core fibers *Light Sci. Appl.* **6** e17124
[23] Jeong Y-G *et al* 2018 Direct compression of 170-fs 50-cycle pulses down to 1.5 cycles with 70% transmission *Sci. Rep.* **8** 1–6
[24] Adamu A I, Habib M S, Petersen C R, Lopez J E A, Zhou B, Schülzgen A, Bache M, Amezcua-Correa R, Bang O and Markos C 2019 Deep-UV to mid-IR supercontinuum generation driven by mid-IR ultrashort pulses in a gas-filled hollow-core fiber *Sci. Rep.* **9** 1–9
[25] Rampur A *et al* 2020 Temporal fine structure of all-normal dispersion fiber supercontinuum pulses caused by non-ideal pump pulse shapes *Opt. Express* **28** 16579–93
[26] Wirth A *et al* 2011 Synthesized light transients *Science* **334** 195–200
[27] Hassan M T, Wirth A, Grguraš I, Moulet A, Luu T T, Gagnon J, Pervak V and Goulielmakis E 2012 Invited article: attosecond photonics: synthesis and control of light transients *Rev. Sci. Instrum.* **83** 111301
[28] Schultze M *et al* 2014 Attosecond band-gap dynamics in silicon *Science* **346** 1348–52
[29] Hassan M T *et al* 2016 Optical attosecond pulses and tracking the nonlinear response of bound electrons *Nature* **530** 66–70
[30] Wilson D J, Ren X, Zigo S, Légaré F and Trallero-Herrero C 2018 Simultaneous few-cycle pulse generation of the depleted pump and signal from an optical parametric amplifier *J. Opt. Soc. Am.* B **35** A45–A48
[31] Shan B and Chang Z 2001 Dramatic extension of the high-order harmonic cutoff by using a long-wavelength driving field *Phys. Rev.* A **65** 011804
[32] Colosimo P *et al* 2008 Scaling strong-field interactions towards the classical limit *Nat. Phys.* **4** 386–9
[33] Keiber S, Sederberg S, Schwarz A, Trubetskov M, Pervak V, Krausz F and Karpowicz N 2016 Electro-optic sampling of near-infrared waveforms *Nat. Photon.* **10** 159–62
[34] Park S B, Kim K, Cho W, Hwang S I, Ivanov I, Nam C H and Kim K T 2018 Direct sampling of a light wave in air *Optica* **5** 402–8
[35] Cho W, Hwang S I, Nam C H, Bionta M R, Lassonde P, Schmidt B E, Ibrahim H, Légaré F and Kim K T 2019 Temporal characterization of femtosecond laser pulses using tunneling ionization in the UV, visible, and mid-IR ranges *Sci. Rep.* **9** 16067
[36] Kane D J and Trebino R 1993 Characterization of arbitrary femtosecond pulses using frequency-resolved optical gating *IEEE J. Quantum. Electron.* **29** 571–9
[37] Iaconis C and Walmsley I A 1998 Spectral phase interferometry for direct electric-field reconstruction of ultrashort optical pulses *Opt. Lett.* **23** 792–4
[38] Miranda M, Arnold C L, Fordell T, Silva F, Alonso B, Weigand R, L'Huillier A and Crespo H 2012 Characterization of broadband few-cycle laser pulses with the d-scan technique *Opt. Express* **20** 18732–43
[39] Witting T, Greening D, Walke D, Matia-Hernando P, Barillot T, Marangos J P and Tisch J W G 2016 Time-domain ptychography of over-octave-spanning laser pulses in the single-cycle regime *Opt. Lett.* **41** 4218–21
[40] Imran T, Hussain M and Figueira G 2016 Cross-correlation frequency-resolved optical gating of white-light continuum (500–900 nm) generated in bulk media by 1053 nm laser pulses *Laser Phys. Lett.* **13** 066101
[41] Fan G, Balčiūnas T, Fourcade-Dutin C, Haessler S, Voronin A A, Zheltikov A M, Gérôme F, Benabid F, Baltuška A and Witting T 2016 X-SEA-F-SPIDER characterization of over octave spanning pulses in the infrared range *Opt. Express* **24** 12713–29
[42] Krogen P, Suchowski H, Liang H, Flemens N, Hong K H, Kärtner F X and Moses J 2017 Generation and multi-octave shaping of mid-infrared intense single-cycle pulses *Nat. Photon.* **11** 222–6
[43] Miranda M *et al* 2019 All-optical measurement of the complete waveform of octave-spanning ultrashort light pulses *Opt. Lett.* **44** 191–4
[44] Brahms C, Belli F and Travers J C 2020 Infrared attosecond field transients and UV to IR few-femtosecond pulses generated by high-energy soliton self-compression *Phys. Rev. Res.* **2** 043037
[45] Leblanc A *et al* 2019 Phase-matching-free pulse retrieval based on transient absorption in solids *Opt. Express* **27** 29015
[46] Cilento F, Giannetti C, Ferrini G, Dal Conte S, Sala T, Coslovich G, Rini M, Cavalleri A and Parmigiani F 2010 Ultrafast insulator-to-metal phase transition as a switch to measure the spectrogram of a supercontinuum light pulse *Appl. Phys. Lett.* **96** 021102
[47] Wegkamp D, Brida D, Bonora S, Cerullo G, Stähler J, Wolf M and Wall S 2011 Phase retrieval and compression of low-power white-light pulses *Appl. Phys. Lett.* **99** 101101

[48] Itakura R, Kumada T, Nakano M and Akagi H 2015 Frequency-resolved optical gating for characterization of VUV pulses using ultrafast plasma mirror switching *Opt. Express* **23** 10914–24
[49] Itakura R, Akagi H and Otobe T 2019 Characterization of 20-fs VUV pulses by plasma-mirror frequency-resolved optical gating *Appl. Phys. Lett.* **44** 2282–5
[50] Schmidt B E *et al* 2010 Compression of 1.8 μm laser pulses to sub two optical cycles with bulk material *Appl. Phys. Lett.* **96** 121109
[51] Petersen C R *et al* 2014 Mid-infrared supercontinuum covering the 1.4–13.3 μm molecular fingerprint region using ultra-high NA chalcogenide step-index fibre *Nat. Photon.* **8** 830–4